ARTICLES

Excited-State Intramolecular Proton Transfer in 2-(2′-Tosylaminophenyl)benzimidazole

Christoph J. Fahrni,* Maged M. Henary, and Donald G. VanDerveer

School of Chemistry of Biochemistry, Georgia Institute of Technology, 770 State Street, Atlanta, Georgia 30332

Received: February 21, 2002; In Final Form: April 30, 2002

The spectroscopic properties of 2-(2′-tosylaminophenyl)benzimidazole (TPBI) have been studied in a series of different solvents. As revealed by absorbance, steady-state, and time-resolved emission spectroscopy, the molecule undergoes fast excited-state intramolecular proton transfer (ESIPT) to yield emission of the corresponding tautomeric species with a large quantum yield (0.5). The fluorescence emission shows monoexponential decay kinetics ($\tau = 4.5$ ns) regardless of the nature of the solvent. The ground-state equilibrium is dominated by a single rotamer and small amounts of the deprotonated anion. The X-ray structure of TPBI shows a substantial out-of-plane twist along the aryl−benzimidazole bond axis, which is presumably due to π-stacking interactions between the tosylamide and benzimidazole rings. Ab initio calculations suggest a different structure in the gas phase without π-stacking interactions and a substantially reduced twist angle. A large energy barrier for interconversion of the cis- and trans-rotamers in the ground and excited state has been predicted on the basis of DFT calculations, which is in agreement with all experimental data. The ground-state equilibrium and ESIPT process of TPBI are essentially unaffected by the nature of the solvent, which is of particular interest to sensing applications in cell biology.

Introduction

Excited-state intramolecular proton transfer can be observed in a wide range of molecules and has led to various applications in the form of laser dyes,[1,2] high-energy radiation detectors,[3−5] UV photostabilizers,[6,7] or fluorescent probes.[8−10] In the case of the adiabatic, barrierless excited-state intramolecular proton transfer (ESIPT), a covalently attached proton, typically of a hydroxyl or amino group, in the electronically excited state migrates to a neighboring hydrogen-bonded atom less than 2 Å away. The phototautomer formed emits light and thermally equilibrates back to the ground state with the proton bound to its original atom. This process can proceed extremely fast and several studies have found subpicosecond reaction rates for a variety of molecules.[11−13] Because the formed phototautomer is more stable in the excited state but not the ground state, the observed Stokes' shift of the fluorescence emission is unusually large.[14]

Among the compound classes exhibiting ESIPT, the photophysics of benzazole derivatives has been investigated extensively.[15−25] Several studies on 2-(2′-hydroxyphenyl)benzothiazole (HPBT), -benzoxazole (HPBO), and -benzimidazole (HPBI) revealed dual emission in polar solvents,[17] which has been attributed to the presence of different species in the ground and excited state. For example, the ground-state equilibrium of HPBI in polar media includes the cis- and trans-rotamers of the enol form (E_c and E_t) as well as the keto tautomer (K) (Scheme 1). In aqueous solution or polar protic solvents the equilibrium is further complicated by the pH-dependent formation of the phenolate anion. It has been shown that only the cis-enol form E_c is able to undergo fast proton transfer in the excited state, resulting in a highly Stokes' shifted emission of the keto tautomer (K*).[26] The observed normal emission bands at higher energy are due to all other species present such as the trans-rotamer E_t, the phenolate anion, and the open cis-enol form, in which the OH group is hydrogen bonded to a solvent molecule rather than to the imidazole nitrogen.[17] The equilibrium position is strongly influenced by the polarity of the solvent, which in turn determines the ratio of normal and ESIPT emission intensities. For example, in aqueous solution, the high solvent polarity combined with the capacity to form hydrogen bonds interferes with the ESIPT process such that only a weak tautomer emission is observed and the normal emission constitutes the major band.[27] This property has been favorably applied to probing of the microenvironment of large molecules, as described for the interaction of HPBI with a protein.[8,9]

The emission of ESIPT molecules is also responsive toward metal coordination, a property that is of interest for the development of cation sensitive ratiometric fluorescent probes.[27] For such applications, the strong environmental dependence of the emission is undesirable because the probe should only reflect changes in the metal concentration. This is particularly the case for biological applications, in which the probe is exposed to a large range of environments with different polarities, including the cytoplasm, intracellular compartments, or partitioning into membrane bilayers.

Because the polarity responsiveness of HPBI is due to the presence of several species in the ground-state equilibrium, the problem could be eliminated with a molecule that exists only as a single rotamer which can undergo ESIPT. Furthermore, the efficiency of the ESIPT process is influenced not only by

* To whom correspondence should be addressed. Phone: 404-385-1164/ fax: 404-894-2295. E-mail address: fahrni@chemistry.gatech.edu.

10.1021/jp0204915 CCC: $22.00
Published on Web 07/31/2002

SCHEME 1

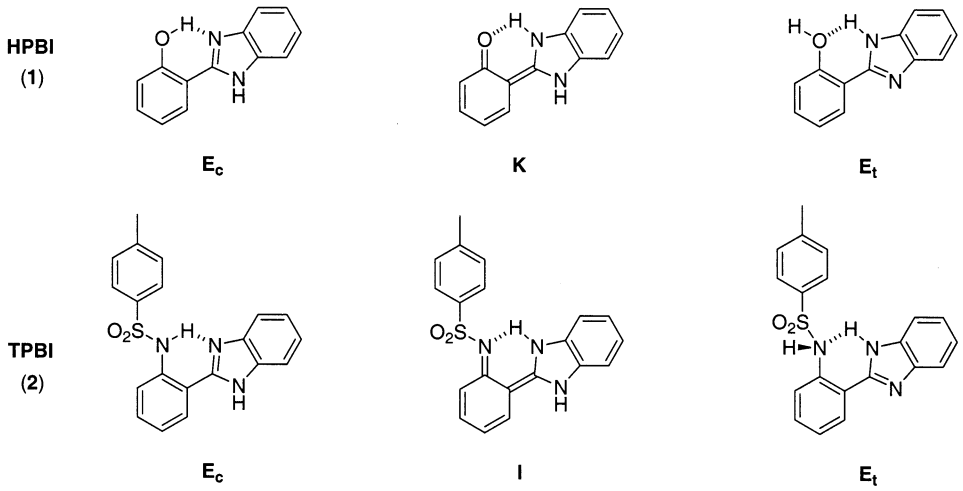

the solvent polarity but also by the p*K* value of the proton, which is shifted in the excited state. With increasing p*K*, the thermodynamics of the excited-state proton transfer become less favorable, resulting in an increased normal emission band.[28−30] Therefore, the p*K* value of the probe should be as low as possible, but still sufficiently high to guarantee protonation of the ground-state species at the pH at which the probe is used.

In this work, we have studied the excited-state intramolecular proton-transfer reaction of 2-(2′-tosylaminophenyl)benzimidazole (TPBI, **2**), which contains a sulfonamide group as the proton donor. In contrast to HPBI, the cis- and trans-rotamers of TPBI (the "enamine form" E_c and E_t) are expected to be very different in energy (Scheme 1). A simple rotation around the carbon−oxygen bond is sufficient to position the lone pair for the formation of the intramolecular hydrogen bond in the trans-rotamer of HPBI (**1**). The analogous structure for TPBI requires rehybridization of the sulfonamide nitrogen, which is accompanied by the loss of resonance stabilization energy between the nitrogen lone pair and the sulfone moiety. Conclusively, the cis-rotamer E_c is substantially favored thermodynamically over the trans-rotamer E_t, and therefore the ground-state equilibrium is expected to be dominated by a single rotamer (E_c). Because the p*K* value of aryl-substituted sulfonamides are comparable to their phenol analogues, the ESIPT process in TPBI is expected to be similarly efficient as for HPBI.

Experimental Section

Materials and Reagents. 2-(2′-Aminophenyl)benzimidazole (Alfa-Aesar, 98%), *p*-toluenesulfonyl chloride (Aldrich, 98%), methanesulfonyl chloride (Aldrich, 98%). NMR: δ in ppm vs $SiMe_4$ (0 ppm, ^{1}H, 300 MHz). MS: selected peaks, *m*/*z*. Melting points are uncorrected. Flash chromatography (FC): Merck silica gel (230−400 mesh). TLC: 0.25 mm, Merck silica gel 60 F254, visualizing at 254 nm or with 2% $KMnO_4$ solution. All solvents used for absorption and fluorescence measurements were of spectroscopic grade.

Synthesis. (a) 2-(2′-Tosylaminophenyl)benzimidazole (2). To a solution of 2-(2′-aminophenyl)benzimidazole (500 mg, 2.39 mmol) in pyridine (7 mL) was added *p*-toluenesulfonyl chloride (478 mg, 2.51 mmol) at room temperature, and the resulting mixture was stirred for 6 h. The mixture was poured into H_2O (10 mL), neutralized with HCl (1M), and extracted with ethyl acetate (3 × 30 mL). The combined organic phase was washed with H_2O (2 × 10 mL), dried with $MgSO_4$, filtered, and concentrated in vacuo, affording a brown oil, which was purified by flash chromatography on silica gel (EtOAc−hexane 1:2 → 1:1) providing 625 mg of the sulfonamide as a colorless solid (1.72 mmol, 72%).

Mp: 164−165 °C. R_f: 0.3 (1:2 hexane:EtOAc). ^{1}H NMR ($CDCl_3$, 300 MHz): δ 2.25 (s, 3H), 6.98−7.08 (m, 3H), 7.18−7.32 (m, 3H), 7.30 (m, 2H), 7.58−7.72 (m, 6H), 9.85 (s, broad, 1H), 13.05 (s, broad, 1H). MS (70 eV): 363 (M^+, 36), 299 (20), 208 (100), 91 (26), 65 (25). EI-HRMS, *m*/*e*: calculated for (M^+) $C_{20}H_{17}N_3O_2S$ 363.10415, found 363.10279.

(b) 2-(2′-Mesylaminophenyl)benzimidazole (3). Prepared as described for compound **2**. Mp: 213-215 °C. R_f: 0.3 (1:2 hexane:EtOAc). ^{1}H NMR (DMSO-d_6, 300 MHz): δ 3.17 (s, 3H), 7.27−7.35 (m, 3H), 7.54 (td, J = 7.7, 1.1 Hz, 1H), 7.62−7.72 (m, 3H), 8.18 (dd, J = 8.24, 1.1 Hz, 1H), 13.09 (s, broad, 2H). MS (70 eV): 287 (M^+, 45). 208 (100), 181 (15), 118 (10), 92 (9), 65 (13). EI-HRMS, *m*/*e*: calculated for (M^+) $C_{14}H_{13}N_3O_2S$ 287.07285, found 287.07237.

Both compounds were purified by semipreparative reversed-phase HPLC (Varian ProStar system with UV detector), 10 mm RP 18 column (acetonitrile−water, gradient 30% → 2% water), eliminating minor impurities (<1%) that were not detectable by TLC or NMR.

Steady-State Absorption and Fluorescence Spectroscopy. All sample stock solutions and buffer solutions were filtered through 0.2 μm Teflon membrane filters to remove interfering dust particles or fibers. UV−vis absorption spectra were recorded at 25 °C using a Varian Cary Bio50 UV−vis spectrometer with a constant-temperature accessory. Steady-state emission and excitation spectra were recorded with a PTI fluorometer and FELIX software. For all measurements the path length was 1 cm with a cell volume of 3.0 mL. All fluorescence spectra have been corrected for the spectral response of the detection system (emission correction file provided by instrument manufacturer) and for the spectral irradiance of the excitation channel (via calibrated photodiode). Quantum yields were determined using quinine sulfate dihydrate in 1 N H_2SO_4 as fluorescence standard ($\Phi_f = 0.54 \pm 0.05$).[31]

Fluorescence Lifetime Measurements. Fluorescence lifetime data were acquired with a Photon Technology International (PTI) fluorescence lifetime instrument. The system uses a nitrogen laser (model GL-3300) as the excitation source combined with a stroboscopic detector. All samples were excited at 337 nm with a repetition rate of 10 Hz (pulse width 3−4 ns), and the fluorescence signal was analyzed after passing through a monochromator set at the peak emission of the corresponding

TABLE 1: Crystallographic Data for 2-(2′-Tosylaminophenyl)benzimidazole (2)

formula	$C_{20}H_{17}N_3O_2S$
molecular weight	363.43
color, habit	colorless
crystal size (mm)	1.02 × 0.07 × 0.07
crystal system	monoclinic
space group	*P*2(1)/*n*
a (Å)	7.3393(7)
b (Å)	17.8290(17)
c (Å)	13.7468(13)
β (deg)	99.842(2)
V (Å^3)	1772.3(3)
Z	4
calculated density (g/cm^3)	1.362
F(000)	760
temp (K)	198(2)
2θ range (deg)	3.78−50.20
no. of reflns collected	3149
no. of indep rflns	1980
final *R* indices (obs data) (%): R,[a] R_w[b]	3.95, 9.02
R indices (all data) (%): R,[a] R_w[b]	7.40, 10.06
goodness of fit on F^2	0.932

[a] $R = \sum||F_o| - |F_c||/\sum|F_o|$. [b] $R_w = (\sum w(|F_o| - |F_c|)^2/\sum w|F_o|^2)^{1/2}$.

sample. The data were analyzed with the TimeMaster Pro software package provided with the spectrometer.

Quantum Chemical Calculations. All calculations were carried out with the Q-Chem electronic structure calculation suite of programs.[32] The geometries of the ground-state structures were optimized by the density functional method using the hybrid B3LYP functional with the split-valence polarized 6-31G* (6-31G(d)) basis set. Excited-state geometries were optimized in the first excited singlet state (S_1) using configuration interaction with all singly excited determinants (CIS)[33] and the 6-31G* basis set. To obtain estimates of the vertical electronic excitation energies that include some account of electron correlation, time-dependent density functional theory (TD-DFT)[34] calculations with the B3LYP functional and 6-31G* basis set were performed. B3-LYP corresponds to the combination of Becke's three parameter exchange functional (B3)[35] with a Lee−Yang−Parr fit for the correlation functional (LYP).[36] Transition energies were also calculated on the basis of the semiempirical ZINDO method[37] using configuration interactions with an active space of 15 occupied and 15 unoccupied molecular orbitals. The calculation of ground-state potential curves is based on relaxed geometries with the corresponding constraints of dihedral angles (for rotations) or bond lengths (reaction coordinate). Excited-state potential curves were computed with the ground-state geometries via TD-DFT calculations as described above (B3LYP/6-31G* basis set).

X-ray Structure Analysis. Crystals of **2** suitable for X-ray structural analysis were grown from dichloromethane solution by isothermal distillation with hexane over the period of 1 week.

A summary of the crystallographic details is given in Table 1. The X-ray data were collected on a Siemens SMART 1K CCD diffractometer with graphite-monochromated Mo Kα radiation (λ = 0.710 73 Å). The programs SADABS (Sheldrick)[38] and SAINT 6.22 (Bruker)[39] were used for absorption corrections. The structure was solved by direct methods and refined by least-squares calculations with the SHELXTL 5.10 software package.[39] The hydrogen atoms were added by using ideal geometries with a fixed C−H bond distance of 0.96 Å.

Results and Discussion

1. Structural Studies. *X-ray Crystallography.* Reaction of 2-(2′-aminophenyl)benzimidazole with *p*-toluenesulfonyl chloride in anhydrous pyridine provided sulfonamide **2** in 72% yield. The compound was crystallized from dichloromethane/hexane and characterized via X-ray analysis. An ORTEP plot of the molecule is shown in Figure 1, and all relevant geometrical parameters are compiled in Table 2. The most striking feature of the structure is the parallel orientation of the tosyl and benzimidazole rings, leading to significant intramolecular π-stacking interactions. The two planes deviate only by 6.6° from a parallel orientation with a distance of approximately 3.3 Å. The unusual geometry is best revealed with a projection along the C2−C7 bond axis (Figure 2), which shows a dihedral angle of 29° between the benzimidazole ring and the attached phenyl ring. The space filling representation in Figure 2 illustrates the close contacts of the two aromatic rings. The substantial out-of-plane twist of the aryl−benzimidazole unit is presumably a result of the π-stacking interaction, which is most effective with a planar orientation of the aryl rings. This assumption is further supported by the geometry reported for 2-(2′-tosylamino-5′-

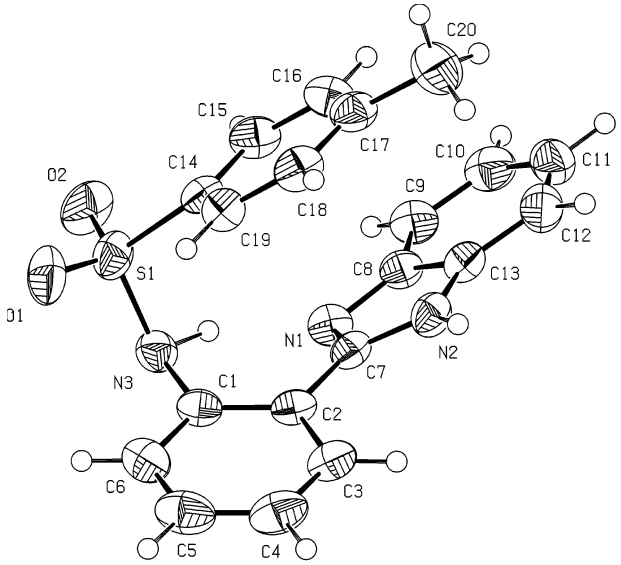

Figure 1. ORTEP plot (50% probability) and atom numbering scheme for the X-ray structure of 2-(2′-tosylaminophenyl)benzimidazole (**2**).

TABLE 2: Selected Experimental and Calculated Structural Data for 2-(2′-Tosylaminophenyl)benzimidazole (2)

parameter[a]	X-ray struct	rotamer E_c[b]	tautomer I* (S_1)[c]
N(1)−C(7) (Å)	1.324(2)	1.324	1.326
N(2)−C(7) (Å)	1.362(3)	1.383	1.348
N(3)−C(1) (Å)	1.444(3)	1.408	1.339
C(2)−C(7) (Å)	1.465(3)	1.465	1.438
C(1)−C(2) (Å)	1.397(3)	1.424	1.429
C(1)−C(6) (Å)	1.379(3)	1.404	1.427
C(5)−C(6) (Å)	1.378(3)	1.390	1.361
C(4)−C(5) (Å)	1.385(4)	1.397	1.410
C(3)−C(4) (Å)	1.374(3)	1.388	1.358
C(2)−C(3) (Å)	1.389(3)	1.407	1.414
C(14)−S(1)−N(3) (deg)	106.59(9)	106.048	106.525
S(1)−N(3)−C(1) (deg)	116.11(13)	124.816	126.525
N(1)−C(7)−N(2) (deg)	112.41(18)	111.332	107.326
N(1)−C(7)−C(2) (deg)	124.9(2)	125.796	126.496
C(1)−C(2)−C(7) (deg)	120.8(2)	121.735	120.309
C(2)−C(1)−N(3) (deg)	120.40(19)	120.091	117.471
C(1)−C(2)−C(7)−N(1) (deg)	−28.637	−14.425	−0.633

[a] Atom numbering scheme shown in Figure 1. [b] Geometry optimized ground-state structure of the cis-rotamer E_c (density functional method with B3LYP functional and 6-31G* basis set). [c] Geometry optimized structure of the sulfonimino tautomer I in the lowest excited singlet state S_1 (Hartree−Fock method with configuration interaction using all singly excited determinants (CIS) and 6-31G* basis set).

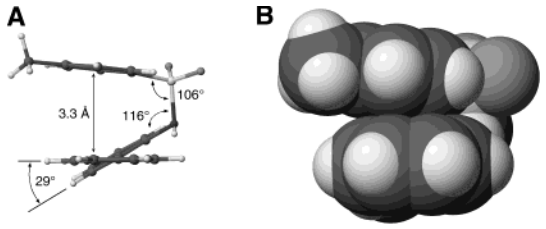

Figure 2. Molecular geometry of **2**: (a) projection along the C2−C7 bond axis; (b) space-filling model showing the π-stacking interaction between the toluene and benzimidazole rings.

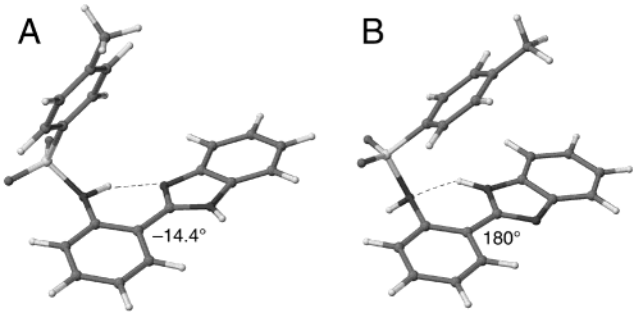

Figure 3. Geometry optimized ground-state structures (B3LYP/6-31G*) for two rotamer conformations of **2**: (a) most stable geometry; (b) geometry with a local energy minimum and a dihedral angle (C1−C2−C7−N1) of 180°.

methylphenyl)benzoxazole, in which the two aryl rings are essentially coplanar with a small dihedral angle of 2.5°.[40] Additional geometric constraints induced by the π-stacking interaction can be observed along the sulfonamide backbone. Whereas the bond angle C14−S1−N3 of 106° is in the typical range for aromatic sulfonamides, the S1−N3−C1 angle of 116° is considerably more acute than 124−125°, which is typically found for similar compounds.[41,42]

Ab Initio Calculations. The observed π-stacking interaction cannot necessarily be translated to the solution phase (or gas phase) and could be due to a packing effect in the solid state. Starting with the coordinates of the X-ray structure, a full DFT geometry optimization with the B3LYP hybrid functional and a 6-31G* basis set was performed. The resulting calculated gas-phase structure revealed a more relaxed geometry without the π-stacking interaction of the two aryl units (Figure 3A). A compilation of the most important geometrical parameters is given in Table 2. In general, the bond lengths and angles of the aromatic rings are in very good agreement with the data obtained from the X-ray structure. The considerably wider angle of 124.8° for S1−N3−C1 reflects the more relaxed geometry that is now within the typical range of arenesulfonamides based on published X-ray structures.[41,42] In addition, the intersecting benzimidazole and phenyl ring planes are substantially less twisted, as reflected by the smaller dihedral angle of −14.4° for C1−C2−C7−N1. Conclusively, the π-stacking interaction might only be important in the solid state, and not in the gas or solution phase.

The topology of the potential energy surface in the ground state has important implications for the emission properties of the molecule. Because only the cis-rotamer E_c undergoes ESIPT, any other rotamer that is present in the ground-state equilibrium will decrease the population of E_c and therefore also decrease the efficiency of the ESIPT process. Whereas in the case of HPBI, several rotational isomers are in thermal equilibrium in the ground state,[17] the sulfonamide analogue TPBI **2** is expected to show significant differences for the stability of the cis- and trans-rotamers (vide supra). A relaxed potential energy surface

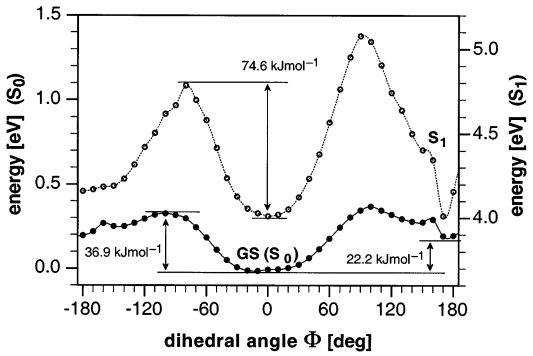

Figure 4. Geometrically relaxed potential energy curves for the ground (S_0) and lowest excited singlet state (S_1) of **2** as a function of the dihedral angle Φ = C1−C2−C7−N1.

was calculated by DFT with the B3LYP hybrid functional (6-31G* basis set) by successive rotation around the C2−C7 bond axis (Figure 4). As expected, the minimum energy conformation with a dihedral angle of −14.4° is substantially more stable than any other rotamer. The calculation revealed only one additional local minimum with significant stability, which corresponds to the conformer with a dihedral angle of 180° (Figure 3B). This structure is 22.2 kJ mol^{-1} less stable compared to the minimum energy conformation, which can mostly be attributed to the loss of resonance stabilization energy upon pyramidalization of the sulfonamide nitrogen atom. The estimated activation energy for the interconversion between the two conformers is 36.9 kJ mol^{-1}. On the basis of the Maxwell−Boltzmann distribution function, the populations of the cis- and trans-rotamers at 298 K in the gas phase can be calculated to be 0.99987/0.00013. Even though the absolute energies estimated for the gas-phase structures might vary in solution due to dipolar solvent stabilization, the stability difference between the cis- and trans-isomers is considerable and is expected to simplify the ground-state equilibrium.

2. Photophysical Studies. *Absorption Spectra.* The absorption spectra of compound **2** were measured in different solvents (Figure 5). Regardless of the solvent polarity, all spectra show a distinct vibrational structure, which is indicative of a considerably rigid molecular framework. Presumably, the two aromatic rings of the phenyl−benzimidazole unit are in a coplanar orientation, which is effectively stabilized by the strong intramolecular hydrogen bond between the sulfonamide NH group and the imidazole nitrogen.

The peak absorption wavelength undergoes only a slight hypsochromic shift from 319 to 314 nm with increasing solvent polarity (Table 3). The close similarity of all spectra indicates that the ground-state structure of **2** must be very similar in all solvents. Even in protic and very polar solvents such as MeOH or EtOH, no significant changes were observed that might imply the presence of an additional ground-state conformation or rotamer. Apparently, the cis-rotamer E_c is the most stable structure not only in the gas phase, as suggested by the DFT prediction, but also in solution phase. The molar absorption coefficients range between 14 000 to 20 000 cm^{-1} M^{-1}, which is in the typical range for allowed $\pi-\pi^*$ transitions. The nature of the $S_0 \rightarrow S_1$ electronic transition was further confirmed by quantum chemical calculations (vide infra). Another interesting feature is the weak but significant absorption band above 350 nm, which was only observed in polar protic solvents as well as in acetonitrile (Figure 5a). Mosquera et al. observed a similar weak band in the absorption spectra for HPBI (**1**) and suggested the presence of the keto-tautomer K in the ground-state equilibrium.[17] Another possibility might include the presence

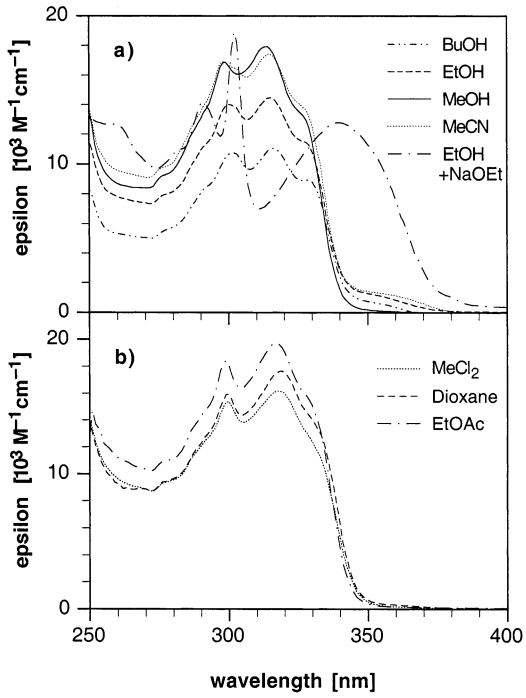

Figure 5. UV−vis absorption spectra for 2-(2′-tosylaminophenyl)benzimidazole (**2**) in various solvents at 298 K.

TABLE 3: UV-vis Spectral Data (Absorption Maxima and Extinction Coefficients) for 2-(2′-Tosylaminophenyl)benzimidazole (2) in Various Solvents at 298 K

solvent	λ_{max} (nm)	ϵ_{max} (M^{-1} cm^{-1})	λ_{max} (nm)	ϵ_{max} (M^{-1} cm^{-1})
cyclohexane (sat)	300		318	
dioxane	300	15900	319	17600
diethyl ether	299	16600	318	17800
dichloromethane	300	15400	318	15400
ethyl acetate	299	18400	317	19700
acetonitrile	299	16900	315	17400
tetrahydrofuran	300	15600	318	17000
n-butanol	302	12000	316	12300
ethanol	300	13300	315	13900
methanol	299	16900	314	17900
EtOH/NaOEt	302	20700	341	14100

of small amounts of deprotonated ground-state anion, as suggested by Douhal et al. for 2-(2′-hydroxyphenyl)imidazole and 2-(2′-hydroxyphenyl)benzimidazole (**1**).[43] In case of HPBI the latter possibility was excluded on the basis of the absorption spectrum of the deprotonated dye, which does not show an absorption band in the low-energy wavelength region.[17] Addition of sodium ethoxide to a solution of TPBI in ethanol yielded a red-shifted absorption band with a maximum at 340 nm (Figure 5a). The weak low-energy band observed in neutral ethanol matches well with this absorption band and therefore is consistent with the presence of small amounts of deprotonated anion. Further evidence for this interpretation was found by the steady-state fluorescence data, as illustrated below.

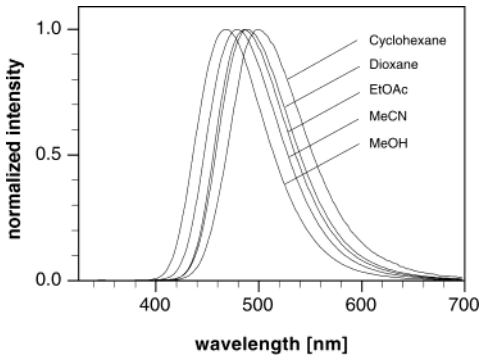

Figure 6. Normalized fluorescence emission spectra for 2-(2′-tosylaminophenyl)benzimidazole (**2**) in various solvents at 298 K.

Fluorescence Steady-State Spectra. The fluorescence spectral data of TPBI (**2**) were measured in the same solvent set used for the absorption spectra and are compiled in Table 4. In all solvents, a strongly Stokes' shifted emission band was observed, which can presumably be attributed to the sulfonimino tautomer I* (Scheme 1). Initial measurements showed a weak emission band at higher energy in most solvents, which we interpreted with the presence of the trans-rotamer E_t. Nevertheless, as quantum chemical calculations suggested, the ground-state equilibrium should be exclusively dominated by the cis-rotamer E_c, and therefore the normal emission band was a surprising observation. Careful analysis of the compound by analytical reversed-phase HPLC revealed a small amount of impurity (<1%), which we were not able to detect by thin-layer chromatography nor in the proton NMR spectrum. Rigorous purification of a sample by semipreparative reversed-phase HPLC yielded very pure material. As shown in Figure 6, the spectra of the purified sample exhibit a single, clean emission band in all solvents and are lacking the normal emission at higher energy as observed for HPBI derivatives.[17,27] Most importantly, the normalized emission spectra were invariable of the excitation energy in any given solvent. This further supports the presence of a single species that is responsible for the observed emission band. Furthermore, the long wavelength tail in the absorption spectra in polar solvents was still found with the rigorously purified sample and is therefore not due to impurities. These results contrast the data reported for 2-(2′-acetamidophenyl)benzimidazole[30] and 2-(2′-benzamidophenyl)-

TABLE 4: Fluorescence Spectral Data for 2-(2′-Tosylaminophenyl)benzimidazole (2) in Various Solvents at 298 K

solvent	excitation λ_{max} (nm)	emission λ_{max} (nm)	quantum yield[a] Φ_f	lifetime[b] τ (ns)	χ^2 [c]	k_f (10^8 s^{-1})[d]	k_{nr} (10^8 s^{-1})[e]
cyclohexane	319	507	0.53	5.67	1.25	0.93	0.83
dioxane	319	492	0.53	6.42	1.26	0.83	0.73
diethyl ether	317	485	0.58	6.23	1.26	0.93	0.67
dichloromethane	317	489	0.59	6.40	0.83	0.92	0.64
ethyl acetate	316	490	0.49	5.88	1.02	0.83	0.87
acetonitrile	314	480	0.49	6.04	1.14	0.81	0.84
tetrahydrofuran	318	490	0.57	6.03	1.02	0.95	0.71
n-butanol	315	470	0.54	5.68	1.04	0.95	0.81
ethanol	314	470	0.55	5.84	1.01	0.94	0.77
methanol	313	470	0.58	5.59	1.07	1.04	0.75

[a] Quinine sulfate in 1 N H_2SO_4 as reference. [b] Lifetime for monoexponential decay model. [c] Goodness of fit parameter for monoexponential curve fit. [d] Radiative deactivation rate constant ($k_f = \Phi_f/\tau$). [e] Nonradiative deactivation rate constant ($k_{nr} = (1 - \Phi_f)/\tau$).

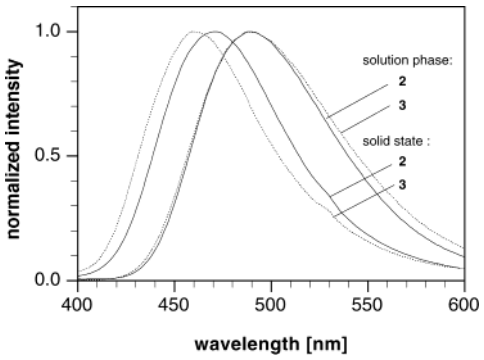

Figure 7. Emission spectra for 2-(2′-tosylaminophenyl)benzimidazole (**2**) and 2-(2′-mesylaminophenyl)benzimidazole (**3**) in solution (dichloromethane) and solid state at 298 K.

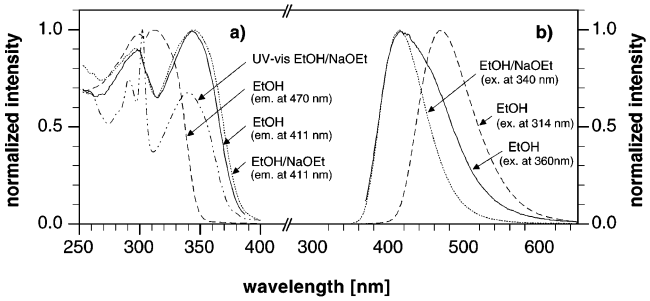

Figure 8. Normalized fluorescence excitation (a) and emission (b) spectra for 2-(2′-tosylaminophenyl)benzimidazole (**2**) in neutral and basic (EtOH/NaOEt) ethanol at 298 K. The indicated wavelengths refer to the emission or excitation wavelength at which the spectra were recorded.

benzimidazole,[29] both of which exhibit dual fluorescence emission in polar solvents.

The peak emission wavelength and Stokes' shift decrease with increasing solvent polarity, suggesting an excited state with a smaller dipole moment compared to the ground state. This observation is consistent with various other ESIPT systems reported in the literature.[30,44] As compared to the phenol analogue HPBI (**1**), the emission is shifted to longer wavelength. For example, in ethanol a peak emission of 450 nm was reported for HPBI (**1**) whereas TPBI (**2**) emits with a maximum of 470 nm.[17] The quantum yields of the tautomer emission in different solvents range between 0.49 and 0.59, which is almost invariable given the experimental error associated with quantum yield measurements. The data are very similar compared to the quantum yields reported for HPBI (0.50-0.65)[43] or 2-(3′-hydroxy-2′-pyridyl)benzimidazole (0.44−0.53),[44] which are also independent of the nature of the solvent.

The excitation spectra are insensitive toward alteration of the emission wavelength at which the spectra were acquired. As illustrated in Table 4, the peak excitation wavelengths are also identical with the measured maxima of the UV spectra. This again is consistent with a single ground-state rotamer, which is responsible for the abnormally Stokes' shifted emission band.

The X-ray structure reveals a π-stacking interaction between the aromatic rings of toluene and benzimidazole, but ab initio optimization of the gas phase geometry suggests a more geometrically relaxed and open structure lacking the π-stacking interaction. Aromatic hydrocarbons quite frequently exhibit excimer fluorescence. Stabilizing interactions between two aromatic rings are possible if one of the two moieties is in an excited state and the HOMO and LUMO of the combined system are only singly occupied. The interplanar separation for excimers of aromatic molecules is typically between 300 and 350 pm and is thus in the same range as the separation of 330 pm observed in the X-ray structure of **2**.[45] If the π-stacking interaction of **2** is also important in solution phase, it should be possible to obtain experimental evidence via comparison of the emission spectra of an aromatic vs an aliphatic sulfonamide derivative. We therefore synthesized the methanesulfonamide analogue **3**, which is lacking the benzene ring required for intramolecular excimer formation. As shown in Figure 7, the solution phase emission spectra of **2** and **3** are virtually identical with a maximum at 489 nm. The interaction of the arenesulfonamide group does not appear to be significant on the basis of these data, which would support an open conformation without π-stacking interaction. This interpretation was further confirmed by the fact that monoexponential fluorescence decay kinetics with very similar lifetimes were observed regardless of the nature of the solvent (vide infra). Interestingly, the emission spectra of **2** and **3** in the solid-state both exhibit a hypsochromic shift, but are not identical (Figure 7). The emission maximum of **2** appears at a longer wavelength with a shift of 10 nm compared to **3**. This indeed would be consistent with an excited-state interaction of the benzimidazole chromophore with the arenesulfonamide group, which results in a more stabilized excited state and therefore a lower emission energy. Because the ESIPT process generates a tautomeric species with an abnormally large Stokes' shifted emission, excited-state interaction via excimer formation is not expected to produce an additional dramatic shift in the emission frequency. Therefore, the observed small differences in the emission spectra support excited-state interactions and are consistent with a π-stacking interaction in the solid state, but not the solution phase.

The steady-state fluorescence data clearly suggest the presence of a single emissive species regardless of the nature of the solvent. Nevertheless, the UV absorption spectra in protic solvents as well as in acetonitrile show an additional weak band above 330 nm, which could be due either to the presence of small amounts of the imino tautomer (**I**, Scheme 1) or the deprotonated sulfonamide anion in the ground-state equilibrium (vide supra). If this weak absorption band originates from the sulfonamide anion, excitation at this wavelength should give rise to normal emission at higher energy. Indeed, when a solution of compound (**2**) in ethanol was excited at 360 nm a very weak blue-shifted emission band with a maximum at 411 nm was observed (Figure 8b). The slight broadening of the band toward longer wavelengths can be attributed to a small contribution of the tautomer emission with a maximum at 470 nm. Addition of excess sodium ethoxide strongly enhances the higher energy band, resulting in a spectrum with an identical maximum at 411 nm. The identification of this species as the deprotonated anion is further supported by the excitation spectrum acquired at 411 nm. In this energy region the intensity of the tautomer emission is approaching zero, therefore, the excitation spectrum should be indicative for the species with an emission maximum at 411 nm. The corresponding normalized excitation spectra measured in neutral and basic ethanol are virtually identical, and their maxima closely match the UV absorption spectrum of the sulfonamide anion (Figure 8a). These data strongly support the presence of small amounts of the deprotonated sulfonamide. Given the close similarity of the weak low-energy band observed not only in ethanol but also in methanol, butanol, and acetonitrile, it is reasonable to assume that in all of these solvents small amounts of deprotonated ligand are present in the ground-state equilibrium.

Time-Resolved Spectroscopy. The time-correlated single photon counting data for the fluorescence decay of TPBI in

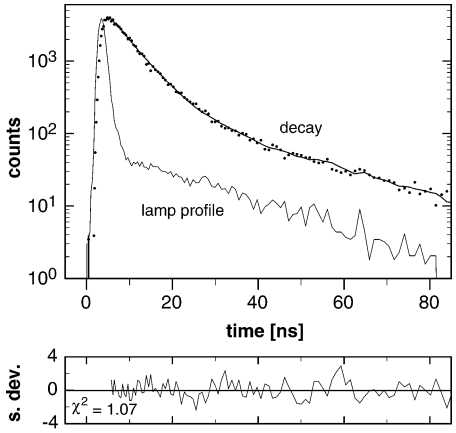

Figure 9. Fluorescence decay data of 2-(2′-tosylaminophenyl)benzimidazole (**2**) in methanol (time-correlated single photon counting). The curve fit is based on a monoexponential decay law ($\tau = 5.59$ ns, $\chi^2 = 1.07$).

methanol is shown in Figure 9. The emission signal fits well to a simple monoexponential decay law with a χ^2 value near unity (1.07). Regardless of the nature of the solvent, the tautomer emission of TPBI revealed monoexponential decay signals without any sign of a biexponential component (Table 4).

Because the only rotamer of TPBI (**2**) detected in the ground state is the cis-conformer E_c, the imino tautomer I* must be formed in the excited state via ESIPT from excited E_c*. Given the instrument resolution of 0.2 ns, the conversion of the cis-rotamer E_c* to I* must occur via ultrafast proton transfer, as has been characterized for various other ESIPT systems including HPBI.[13,16,46,47] The estimated radiative rate constants for the tautomer emission of (**2**) are virtually identical in all solvents used. Similarly, the nonradiative rate constants vary little between the various solvents. The fluorescence lifetime data are consistent with the interpretation of the steady-state spectra and additionally support the presence of a single emissive species in the excited-state manifold.

3. Quantum Chemical Calculations. *Potential Energy Curves.* Calculations of the ground- and excited-state potential curves were carried out using the Q-Chem software package.[32] The ground-state (S_0) geometries were optimized by the density functional method using the B3LYP hybrid functional and a 6-31G* basis set. Excited-state energies were calculated by time-dependent density functional theory (TD-DFT) using the optimized ground-state geometries. All potential energy curves were constructed by variation of the corresponding structural parameter (dihedral angle or bond length) including a full geometry optimization.

As previously indicated in Figure 4, the ground-state potential curve calculated for rotation around the phenyl−benzimidazole bond axis reveals only two stable conformers. The trans-rotamer E_t, corresponding to a dihedral angle of 180°, is considerably higher in energy such that in a thermal equilibrium at room temperature the cis-rotamer E_c will be the predominant species. The energy barrier and relative stability between rotamers can drastically change in the excited state. This might potentially lead to emission from rotamers that are energetically not accessible in the ground-state equilibrium. The approximated first excited-state potential energy curve for rotation around the phenyl−benzimidazole bond axis shows an even greater activation barrier of 74.6 kJ mol^{-1} compared to that of the ground state. Therefore, the interconversion between the cis- and trans-rotamers via an excited-state pathway can be excluded.

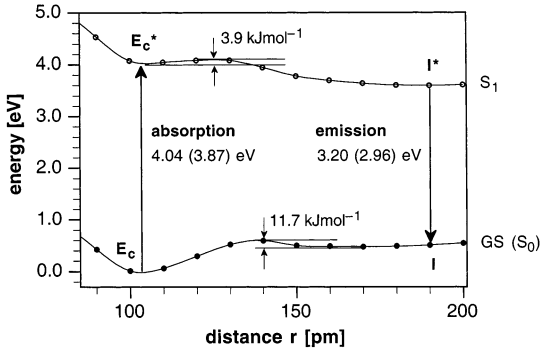

Figure 10. Geometrically relaxed potential energy curves for the ground (S_0) and lowest excited singlet state (S_1) of **2** as a function of the N3−H atom distance (proton-transfer reaction coordinate). Absorption and emission energies are indicated for TD-DFT and CI-ZINDO (in parentheses) calculations.

To investigate the thermodynamics of the ESIPT process in TPBI **2**, the potential energy curves for the ground and first excited singlet state were calculated as a function of the N−H bond length (Figure 10). Whereas the interconversion between the cis- and trans-rotamers is energetically unfavorable in the ground state as well as excited state, the calculated potential energy curve for proton transfer in the excited state is almost barrierless (3.9 kJ mol^{-1}). Thermal equilibration of the tautomer to the ground-state amide tautomer also occurs with a low barrier of 11.7 kJ mol^{-1}.

The optimized excited-state structure of the tautomer (I) shows a distinctly different geometry compared to the computed ground-state structure of **2** (Table 2). An interesting feature is the coplanar orientation of the phenyl−benzimidazole rings with a very small dihedral angle of −0.633°. The excited-state potential energy curve of the enamine rotamer also reaches minimum energy at a coplanar geometry, such that the rotation around the C2−C7 bond axis might already occur prior to the proton-transfer process. Whereas the ground-state structure of **2** shows almost equal bond lengths for all C−C bonds in the central aryl ring, the excited-state tautomer I* exhibits significant differences. The computed bond lengths of the phenyl ring differ by approximately 7 pm and clearly reflect the cross-conjugated nature of the delocalized π-electron system in I*. For the same reason the C2−C7 and C1−N3 bonds are contracted by 4−6 pm compared to the ground-state structure, whereas the N1−C7 is slightly elongated (Table 2).

The potential energy calculations are in agreement with all experimental data, which suggest a single enamine rotamer (E_c) in the ground state. Upon excitation, E_c undergoes ultrafast intramolecular proton transfer to yield the emissive tautomeric imino form I*.

$S_0 \rightarrow S_1$ Vertical Excitation and $S_0 \leftarrow S_1$ Emission Energies. The gas-phase vertical excitation energy for the cis-rotamer E_c of **2** was calculated by the TD-DFT method using the B3LYP hybrid functional and the split-valence polarized 6-31G* basis set. Recent work by Stratmann et al.[34] has shown that time-dependent density functional theory yields significantly better results compared to Hartree−Fock based methods such as the random-phase approximation (RPA) or CIS. A comparison of the computed excitation energy shows a reasonably good prediction with a deviation of 0.1 eV (Table 5). Using the geometries obtained from the DFT optimization the excitation energy was also computed with the configuration interaction approach as implemented in the semiempirical method ZINDO.[37] The CI-ZINDO results given in Table 5 demonstrate the

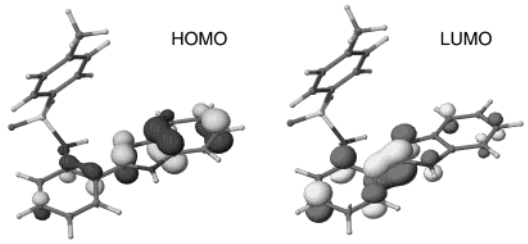

Figure 11. Molecular orbital surfaces of the HOMO and LUMO responsible for the lowest energy transition in the UV−vis spectrum of **2** (CI-ZINDO calculation).

TABLE 5: Experimental and Computed Vertical Excitation Energy (eV) for the Cis-Rotamer E_c and Emission Energy (eV) for the Tautomer I*

method	E_c	I*
TD-DFT (B3LYP/6-31G*)	4.04	3.20
CI-ZINDO	3.87	2.96
Expt	3.94−3.88	2.44−2.64

usefulness of semiempirical methods. The predicted excitation energy is virtually identical compared to the experimental values.

Similarly, the computed TD-DFT energies for the emission of the tautomer I* formed upon proton transfer in the excited state shows a lower but still reasonable correlation with the experimental value. The CI-ZINDO result is in better agreement by about 0.2 eV but still predicts an emission energy that is blue-shifted by 0.4 eV compared to the experimental data (Table 5). Solvent stabilization effects combined with the inaccuracy of the Hartree−Fock CI geometry of the excited state might account for the overestimation of the emission energies. As expected on the basis of the large molar absorption coefficient, the vertical excitation corresponds to a $\pi-\pi^*$ transition. The molecular orbital surfaces of the HOMO and LUMO orbitals involved in the lowest energy transition $S_0 \rightarrow S_1$ is shown in Figure 11 and illustrates the locally excited-state character of the S_1 state. The HOMO exhibits distinctly larger coefficients at the benzimidazole ring. In the excited state (S_1) the HOMO will be singly occupied, resulting an overall electron deficient benzimidazole ring that might undergo interaction with the sulfonamide aryl ring to give rise to excimer formation, as indicated by the solid-state emission spectrum. Presumably, in solution the bond strain energy required to sufficiently approach the two rings is higher than the stabilization energy gained by the interaction to form the excimer.

In summary, both semiempirical CI-ZINDO and TD-DFT computational methods appear to be useful for the prediction of the excitation and emission energies for ESIPT systems based on benzazole derivatives.

Conclusions

TPBI (**2**) exhibits similar photophysical properties as described for the extensively studied and characterized HPBI family of compounds. The latter can undergo facile interconversion between the cis- and trans-rotamers E_c and E_t, and therefore result in a ground-state equilibrium that is strongly dependent on the polarity of the environment. In contrast, the cis-rotamer E_c of TPBI (**2**) is thermodynamically substantially favored over the trans-rotamer E_t, because the interconversion requires rehybridization of the sulfonamide nitrogen accompanied by loss of resonance stabilization energy. Therefore the ground-state equilibrium of TPBI (**2**) is dominated by a single species. All acquired experimental data strongly support this notion. Most important, the ground-state equilibrium and ESIPT process of TPBI are essentially unaffected by the nature of the solvent, which is of particular interest to sensing applications in cell biology.

Acknowledgment. Financial support via startup funds from the Georgia Institute of Technology is gratefully acknowledged. Computations were supported by the Center for Computational Molecular Science and Technology at the Georgia Institute of Technology and partially funded through a Shared University Research (SUR) grant from IBM and the Georgia Institute of Technology. We also thank S. Shealy and D. Bostwick for mass spectral data, Dr. David Sherrill for helpful discussions, Dr. Mostafa El-Sayed for access to the fluorescence lifetime spectrometer, and J. Cody and B. Ayres for a critical review of the manuscript.

Supporting Information Available: Crystallographic data for the structural analysis have been deposited with the Cambridge Crystallographic Data Centre (CCDC 188405). Copies of this information may be obtained free of charge from The Director, CCDC, 12 Union Road, Cambridge CB21EZ, UK (Fax: +44-1223-336033; e-mail: deposit@ccdc.cam.ac.uk or www: http://www.ccdc.cam.ac.uk).

References and Notes

(1) Parthenopoulos, D. A.; McMorrow, D.; Kasha, M. *J. Phys. Chem.* **1991**, *95*, 2668.
(2) Chou, P. T.; Martinez, M. L.; Clements, J. H. *Chem. Phys. Lett.* **1993**, *204*, 395.
(3) Sytnik, A.; Kasha, M. *Radiat. Phys. Chem.* **1993**, *41*, 331.
(4) Chou, P. T.; Martinez, M. L. *Radiat. Phys. Chem.* **1993**, *41*, 373.
(5) Renschler, C. L.; Harrah, L. A. *Nucl. Instrum. Methods Phys. Res., Sect. A* **1985**, *A235*, 41.
(6) Keck, J.; Kramer, H. E. A.; Port, H.; Hirsch, T.; Fischer, P.; Rytz, G. *J. Phys. Chem.* **1996**, *100*, 14468.
(7) O'Connor, D. B.; Scott, G. W.; Coulter, D. R.; Yavrouian, A. *J. Phys. Chem.* **1991**, *95*, 10252.
(8) Sytnik, A.; Kasha, M. *Proc. Natl. Acad. Sci. U.S.A.* **1994**, *91*, 8627.
(9) Sytnik, A.; Gormin, D.; Kasha, M. *Proc. Natl. Acad. Sci. U.S.A.* **1994**, *91*, 11968.
(10) Sytnik, A.; Del Valle, J. C. *J. Phys. Chem.* **1995**, *99*, 13028.
(11) Frey, W.; Elsaesser, T. *Chem. Phys. Lett.* **1992**, *189*, 565.
(12) Marks, D.; Prosposito, P.; Zhang, H.; Glasbeek, M. *Chem. Phys. Lett.* **1998**, *289*, 535.
(13) Barbara, P. F.; Walsh, P. K.; Brus, L. E. *J. Phys. Chem.* **1989**, *93*, 29.
(14) Nagaoka, S.; Kusunoki, J.; Fujibuchi, T.; Hatakenaka, S.; Mukai, K.; Nagashima, U. *J. Photochem. Photobiol. A* **1999**, *122*, 151.
(15) Frey, W.; Laermer, F.; Elsaesser, T. *J. Phys. Chem.* **1991**, *95*, 10391.
(16) Das, K.; Sarkar, N.; Majumdar, D.; Bhattacharyya, K. *Chem. Phys. Lett.* **1992**, *198*, 443.
(17) Mosquera, M.; Penedo, J. C.; Ríos Rodríguez, M. C.; Rodríguez-Prieto, F. *J. Phys. Chem.* **1996**, *100*, 5398.
(18) Roberts, E. L.; Dey, J.; Warner, I. M. *J. Phys. Chem. A* **1997**, *101*, 5296.
(19) Sinha, H. K.; Dogra, S. K. *Chem. Phys.* **1986**, *102*, 337.
(20) Grellmann, K. H.; Mordzinski, A.; Heinrich, A. *Chem. Phys.* **1989**, *136*, 201.
(21) Itoh, M.; Fujiwara, Y. *J. Am. Chem. Soc.* **1985**, *107*, 1561.
(22) Nagaoka, S.; Itoh, A.; Mukai, K.; Hoshimoto, E.; Hirota, N. *Chem. Phys. Lett.* **1992**, *192*, 532.
(23) Stephan, J. S.; Grellmann, K. H. *J. Phys. Chem.* **1995**, *99*, 10066.
(24) Elsaesser, T.; Schmetzer, B.; Lipp, M.; Baeuerle, R. J. *Chem. Phys. Lett.* **1988**, *148*, 112.
(25) Tanaka, K.; Deguchi, M.; Yamaguchi, S.; Yamada, K.; Iwata, S. *J. Heterocycl. Chem.* **2001**, *38*, 131.
(26) Stephan, J. S.; Rodriguez, C. R.; Grellmann, K. H.; Zachariasse, K. A. *Chem. Phys.* **1994**, *186*, 435.
(27) Henary, M. M.; Fahrni, C. J. *J. Phys. Chem. A* **2002**, *106*, 5210.
(28) Santra, S.; Dogra, S. K. *Chem. Phys.* **1998**, *226*, 285.
(29) Santra, S.; Krishnamoorthy, G.; Dogra, S. K. *Chem. Phys. Lett.* **1999**, *311*, 55.
(30) Santra, S.; Krishnamoorthy, G.; Dogra, S. K. *J. Phys. Chem. A* **2000**, *104*, 476.
(31) Demas, J. N.; Crosby, G. A. *J. Phys. Chem.* **1971**, *75*, 991.

(32) Kong, J.; White, C. A.; Krylov, A. I.; Sherrill, C. D.; Adamson, R. D.; Furlani, T. R.; Lee, M. S.; Lee, A. M.; Gwaltney, S. R.; Adams, T. R.; Ochsenfeld, C.; Gilbert, A. T. B.; Kedziora, G. S.; Rassolov, V. A.; Maurice, D. R.; Nair, N.; Shao, Y.; Besley, N. A.; Maslen, P. E.; Dombroski, J. P.; Dachsel, H.; Zhang, W. M.; Korambath, P. P.; Baker, J.; Byrd, E. F. C.; Voorhis, T. V.; Oumi, M.; Hirata, S.; Hsu, C. P.; Ishikawa, N.; Florian, J.; Warshel, A.; Johnson, B. G.; Gill, P. M. W.; Head-Gordon, M.; Pople, J. A. *Q-Chem*; 2.0 ed.; Q-Chem Inc.: CITY, PA, 2000.

(33) Foresman, J. B.; Head-Gordon, M.; Pople, J. A.; Frisch, M. J. *J. Phys. Chem.* **1992**, *96*, 6.

(34) Stratmann, R. E.; Scuseria, G. E.; Frisch, M. J. *J. Chem. Phys.* **1998**, *109*, 8218.

(35) Becke, A. D. *J. Chem. Phys.* **1993**, *98*, 5648.

(36) Lee, C. T.; Yang, W. T.; Parr, R. G. *Phys. Rev. B* **1988**, *37*, 785.

(37) Bacon, A. D.; Zerner, M. C. *Theor. Chim. Acta* **1979**, *53*, 21.

(38) Blessing, R. H. *Acta Crystallogr. Sect. A* **1995**, *51*, 33.

(39) Bruker AXS, Madison, WI, 1998.

(40) Starikova, Z. A.; Obodovskaya, A. E.; Bolotin, B. M. *Zh. Strukt. Khim.* **1982**, *23*, 128.

(41) Bock, H.; Nagel, N.; Nather, C. *Chem. Eur. J.* **1999**, *5*, 2233.

(42) Mahia, J.; Maestro, M.; Vazquez, M.; Bermejo, M. R.; Gonzalez, A. M.; Maneiro, M. *Acta Crystallogr. Sect. C* **1999**, *55*, 2158.

(43) Douhal, A.; Amatguerri, F.; Lillo, M. P.; Acuna, A. U. *J. Photochem. Photobiol. A* **1994**, *78*, 127.

(44) Prieto, F. R.; Rodríguez, M. C. R.; Gonzalez, M. M.; Fernández, M. A. R. *J. Phys. Chem.* **1994**, *98*, 8666.

(45) Klessinger, M.; Michl, J. *Excited States and Photochemistry of Organic Molecules*; VCH: New York, 1995.

(46) Lochbrunner, S.; Wurzer, A. J.; Riedle, E. *J. Chem. Phys.* **2000**, *112*, 10699.

(47) Lochbrunner, S.; Schultz, T.; Schmitt, M.; Shaffer, J. P.; Zgierski, M. Z.; Stolow, A. *J. Chem. Phys.* **2001**, *114*, 2519.